A SECOND ORDER WELL-BALANCED FINITE VOLUME SCHEME FOR EULER EQUATIONS WITH GRAVITY

PRAVEEN CHANDRASHEKAR[†] AND CHRISTIAN KLINGENBERG[‡]

Abstract. We present a novel well-balanced second order Godunov-type finite volume scheme for compressible Euler equations with gravity. The well-balanced property is achieved by a specific combination of source term discretization, hydrostatic reconstruction and numerical flux that exactly resolves stationary contacts. The scheme is able to preserve isothermal and polytropic stationary solutions upto machine precision. It is applied on several examples using the numerical flux of Roe to demonstrate its well-balanced property and the improved resolution of small perturbations around the stationary solution.

Key words. Finite volume, Euler equations, gravity, well-balanced

AMS subject classifications.

1. Introduction. Conservation laws with gravitational source terms occur in many PDE models like shallow water equations and Euler equations. These equations possess non-trivial stationary solutions which are refered to as *hydrostatic* solutions in the case of Euler equations. Euler equations with gravity are useful models for atmospheric flows and stellar structure simulations in astrophysical applications. The hydrostatic Euler equation takes the form of an ordinary differential equation in which the pressure forces are balanced by the gravitational forces. This precise balancing has to be achieved at the numerical level in order to preserve the stationary solution. Since the gravitational source terms are non-conservative this precise balancing is not easy to achieve in the numerical scheme. Conventional numerical schemes in which the source term may be discretized in a consistent manner are not able to preserve such stationary solutions especially on coarse meshes. This leads to erroneous numerical solutions especially when trying to compute small perturbations around the stationary solution necessitating the need for very fine meshes. However in practical 3-D computations it may not be possible to use very fine meshes. The discretization errors in a non-well-balanced scheme can completely mask the small perturbations. Moreover, even a very high order accurate scheme can lead to wrong prediction of small perturbations if the scheme is not well-balanced [15]. A *well-balanced scheme* is designed so that it maintains the precise balance of pressure and gravitational forces in case of the hydrostatic solution. This enables such schemes to more accurately resolve small perturbations around the stationary solution.

To solve the hydrostatic Euler equations exactly, we have to make additional assumptions, for example, constant temperature or constant entropy or a more general polytropic relation. Most of the existing schemes are constructed to preserve one class of hydrostatic solutions, either isothermal or polytropic. The path integral approach is used to construct a wave propagation algorithm which is well-balanced for isentropic solutions in [8] and isothermal solutions in [9]. A well-balanced WENO finite volume scheme which preserves isothermal hydrostatic solutions is presented in [15] by rewriting the gravitational source terms in an equivalent form that precise balancing. In [6] a second order well-balanced scheme is presented using hydrostatic reconstruction and under the assumption of an isentropic flow, which for an ideal gas obeys the relation $p = K\rho^\gamma$. However an isentropic hydrostatic atmosphere is only neutrally stable [7]. A scheme for ideal, compressible, MHD equations which is well-balanced for non-isothermal hydrostatic solutions under ideal gas model is given in [3] for the case of constant gravitational acceleration. A gas-kinetic scheme which is well-balanced for isothermal stationary solutions is presented in [10].

[†]TIFR Center for Applicable Mathematics, Bangalore, India (praveen@tifrbng.res.in)
[‡]Dept. of Mathematics, Univ. of Würzburg, Germany (klingenberg@mathematik.uni-wuerzburg.de)

Using the source term formulation of [15], a non-staggered central scheme which is well-balanced for isothermal stationary solutions is developed in [14]. Well-balanced schemes that satisfy an approximation to the hydrostatic equations have been developed using the approach of relaxation schemes [2, 1], in which an approximation to the hydrostatic solution is built into the solution of the approximate Riemann solver.

In this paper, we propose a novel second order accurate well-balanced scheme for Euler equations with gravity under the ideal gas assumption. The basic approach we take is a Godunov-type finite volume scheme with reconstruction to achieve higher order accuracy. *The same scheme is automatically well-balanced for both isothermal and polytropic hydrostatic solutions*, i.e., it exactly (upto machine precision) preserves the exact hydrostatic solution and this property is independent of the type of gravitational potential. The proposed scheme involves a special discretization of the source terms which is similar to [15] and a reconstruction scheme that uses scaled variables, combined with a numerical flux which preserves stationary contact waves. The scaled variables are chosen so that the pressure is constant in case of the hydrostatic solution, which is crucial to achieving well-balanced property. The scheme only requires the gravitational potential to be known at the cell centers where the other variables are also located. These properties make it attractive to implement the proposed scheme in production codes which also rely on second order reconstruction schemes and contact-preserving numerical flux functions, which can be done with small modifications to the reconstruction process and source term discretization. In more recent work, the current scheme has also been extended to the case of curvilinear meshes which are useful in some applications, like simulation of stellar interiors. We have also extended the current scheme to general equation of state where we can preserve an approximate hydrostatic solution upto machine precision.

The rest of the paper is organized as follows. Section (2) introduces the 1-D Euler equations and its hydrostatic solutions. Section (3) describes the newly proposed well-balanced scheme in 1-D where we also show that the modified source term discretization we use is second order accurate. Section (4) presents some 1-D numerical results to demonstrate its well-balanced property. Section (5) extends the 1-D scheme to the case of 2-D Cartesian meshes. Section (7) presents some 2-D results and we finally end the paper with some conclusions.

2. 1-D Euler equations with gravity. Consider the system of compressible Euler equations in one dimension which models conservation of mass, momentum and energy and are given by

$$\begin{aligned}
\frac{\partial \rho}{\partial t} + \frac{\partial}{\partial x}(\rho u) &= 0 \\
\frac{\partial}{\partial t}(\rho u) + \frac{\partial}{\partial x}(p + \rho u^2) &= -\rho \frac{\partial \phi}{\partial x} \\
\frac{\partial E}{\partial t} + \frac{\partial}{\partial x}(E + p)u &= -\rho u \frac{\partial \phi}{\partial x}
\end{aligned}$$

Here ρ is the density, u is the velocity, p is the pressure, E is the energy per unit volume excluding the gravitational energy and ϕ is the gravitational potential. The pressure is given by

$$p = (\gamma - 1)\left[E - \frac{1}{2}\rho u^2\right], \qquad \gamma = \frac{c_p}{c_v} > 1$$

where γ is the ratio of specific heats at constant pressure and volume, which is taken to be constant. We can write the above set of coupled equations in a compact notation as

$$\frac{\partial \boldsymbol{q}}{\partial t} + \frac{\partial \boldsymbol{f}}{\partial x} = -\begin{bmatrix} 0 \\ \rho \\ \rho u \end{bmatrix} \frac{\partial \phi}{\partial x} \tag{2.1}$$

where $\boldsymbol{q}$ is the set of conserved variables and $\boldsymbol{f}$ is the corresponding flux vector. In the case of self gravitating system, the gravitational potential ϕ is governed by a Poisson-type equation whose details are not relevant for the present discussion. We will consider the case of static gravitational potential which is assumed to be given as a function of the spatial coordinates.

2.1. Hydrostatic states. Consider the hydrostatic stationary solution, i.e., for which the velocity is zero

$$u_e = 0$$

In this case, the mass and energy conservation equations are automatically satisfied. The momentum equation becomes an ordinary differential equation given by

$$\frac{\mathrm{d}p_e}{\mathrm{d}x} = -\rho_e \frac{\mathrm{d}\phi}{\mathrm{d}x} \tag{2.2}$$

Assuming ideal gas and some temperature profile $T_e(x)$

$$p_e(x) = \rho_e(x) R T_e(x)$$

where R is the gas constant, we can integrate the stationary momentum equation (2.2) to obtain

$$p_e(x) = p_0 \exp\left(-\int_{x_0}^{x} \frac{\phi'(s)}{RT_e(s)} \mathrm{d}s \right)$$

In the above equation, p_0 is the pressure at some reference position x_0. If the hydrostatic state is *isothermal*, i.e., $T_e(x) = T_e = \text{const}$, then

$$p_e(x) \exp\left(\frac{\phi(x)}{RT_e} \right) = \text{const} \tag{2.3}$$

If the hydrostatic solution is *polytropic* then we have following relations

$$p_e \rho_e^{-\nu} = \text{const}, \qquad p_e T_e^{-\frac{\nu}{\nu-1}} = \text{const}, \qquad \rho_e T_e^{-\frac{1}{\nu-1}} = \text{const} \tag{2.4}$$

where $\nu > 1$ is some constant. Using these polytropic relations in the hydrostatic equation (2.2) and performing an integration, we obtain

$$\frac{\nu R T_e}{\nu - 1} + \phi = \text{const} \tag{2.5}$$

REMARK 1. *In [6], the authors use the isentropic assumption to show that $h + \phi = \text{const}$ for the hydrostatic solution, where h is the enthalpy. In case of ideal gas, this is identical to equation (2.5) if we take $\nu = \gamma$. However equation (2.5) is more general and includes the polytropic cases for which $\nu \neq \gamma$.*

3. 1-D Finite volume scheme. In order to construct a well-balanced scheme we will first rewrite the gravitational source terms in a specific form by exploiting the structure of the equilibrium solution. To do this, first define*

$$\psi(x) = -\int_{x_0}^{x} \frac{\phi'(s)}{RT(s)} \mathrm{d}s$$

*These quantities are in general time dependent, but to simplify notation we do not explicitly specify the dependance on time.

where x_0 is some arbitrary location. Then

$$\frac{\partial \psi}{\partial x} = -\frac{\partial}{\partial x}\int_{x_0}^{x} \frac{\phi'(s)}{RT(s)}\mathrm{d}s = -\frac{\phi'(x)}{RT(x)} \qquad \text{and} \qquad \frac{\partial}{\partial x}\exp(\psi(x)) = -\exp(\psi(x))\frac{\phi'(x)}{RT(x)}$$

so that

$$-\rho(x)\frac{\partial \phi}{\partial x} = p(x)\exp(-\psi(x))\frac{\partial}{\partial x}\exp(\psi(x)) \tag{3.1}$$

This is a mathematical identity if $\phi'(x)$, $T(x)$ are continuous and it does not depend on the existence of hydrostatic equilibrium. Note that $\psi(x)$ is a continuous function even if $\phi'(x)$ and $T(x)$ are discontinuous. Thus the regularity of the right hand side in (3.1) is no worse than that of the left hand side since ϕ is only continuous in general. We use this transformation to write the gravity source terms in the Euler equations as follows

$$\frac{\partial \boldsymbol{q}}{\partial t} + \frac{\partial \boldsymbol{f}}{\partial x} = \begin{bmatrix} 0 \\ p \\ pu \end{bmatrix} \exp(-\psi(x))\frac{\partial}{\partial x}\exp(\psi(x)) \tag{3.2}$$

Let us divide the domain into N finite volumes each of size Δx. The i'th cell is given by the interval $(x_{i-\frac{1}{2}}, x_{i+\frac{1}{2}})$. Consider the semi-discrete finite volume scheme for the i'th cell

$$\frac{\mathrm{d}\boldsymbol{q}_i}{\mathrm{d}t} + \frac{\hat{\boldsymbol{f}}_{i+\frac{1}{2}} - \hat{\boldsymbol{f}}_{i-\frac{1}{2}}}{\Delta x} = \mathrm{e}^{-\psi_i}\left(\frac{\mathrm{e}^{\psi_{i+\frac{1}{2}}} - \mathrm{e}^{\psi_{i-\frac{1}{2}}}}{\Delta x}\right)\begin{bmatrix} 0 \\ p_i \\ p_i u_i \end{bmatrix} \tag{3.3}$$

where ψ_i, $\psi_{i+\frac{1}{2}}$ etc. are consistent approximations to the function $\psi(x)$ and the consistent numerical flux $\hat{\boldsymbol{f}}_{i+\frac{1}{2}} = \hat{\boldsymbol{f}}(\boldsymbol{q}^L_{i+\frac{1}{2}}, \boldsymbol{q}^R_{i+\frac{1}{2}})$ is assumed to satisfy the following property.

Contact Property *The numerical flux $\hat{\boldsymbol{f}}$ is said to satisfy contact property if for any two states $\boldsymbol{q}^L = [\rho^L, 0, p/(\gamma-1)]$ and $\boldsymbol{q}^R = [\rho^R, 0, p/(\gamma-1)]$ we have*

$$\hat{\boldsymbol{f}}(\boldsymbol{q}^L, \boldsymbol{q}^R) = [0, p, 0]^\top$$

The states $\boldsymbol{q}^L$, $\boldsymbol{q}^R$ in the above definition correspond to a stationary contact discontinuity. The above property is equivalent to the ability of a numerical flux to exactly support a stationary contact discontinuity. Some examples of numerical fluxes which satisfy this property are the Roe flux [11] and the HLLC flux [13].

To obtain the states $\boldsymbol{q}^L_{i+\frac{1}{2}}, \boldsymbol{q}^R_{i+\frac{1}{2}}$ at the cell boundary which are required to calculate the flux $\hat{\boldsymbol{f}}_{i+\frac{1}{2}}$, we will reconstruct the following set of variables

$$\boldsymbol{w} = \left[\rho \mathrm{e}^{-\psi},\ u,\ p\mathrm{e}^{-\psi}\right]^\top$$

Once $\boldsymbol{w}^L_{i+\frac{1}{2}}$ etc. are computed, the primitive variables are obtained as

$$\rho^L_{i+\frac{1}{2}} = \mathrm{e}^{\psi_{i+\frac{1}{2}}}(w_1)^L_{i+\frac{1}{2}}, \qquad u^L_{i+\frac{1}{2}} = (w_2)^L_{i+\frac{1}{2}}, \qquad p^L_{i+\frac{1}{2}} = \mathrm{e}^{\psi_{i+\frac{1}{2}}}(w_3)^L_{i+\frac{1}{2}}, \quad \text{etc.}$$

More details on the reconstruction step are given in section (3.3).

3.1. Well-balanced property. We now state the basic result on the well-balanced property. The case of isothermal and polytropic stationary solutions are identified after the source term discretization is explained since this requires a specific form of discretization.

THEOREM 3.1. *The finite volume scheme (3.3) together with a numerical flux which satisfies* contact property *and reconstruction of* $\boldsymbol{w}$ *variables is well-balanced in the sense that the initial condition given by*

$$u_i = 0, \qquad p_i \exp(-\psi_i) = \text{const}, \qquad \forall\ i \tag{3.4}$$

is preserved by the numerical scheme.

Proof: Let us start the computations with an initial condition that satisfies (3.4). Since we reconstruct the variables $\boldsymbol{w}$, at any interface $i + \frac{1}{2}$ we have

$$u^L_{i+\frac{1}{2}} = u^R_{i+\frac{1}{2}} = 0, \qquad p^L_{i+\frac{1}{2}} = p^R_{i+\frac{1}{2}} = p_i \exp(\psi_{i+\frac{1}{2}} - \psi_i) =: p_{i+\frac{1}{2}}$$

and at $i - \frac{1}{2}$

$$u^L_{i-\frac{1}{2}} = u^R_{i-\frac{1}{2}} = 0, \qquad p^L_{i-\frac{1}{2}} = p^R_{i-\frac{1}{2}} = p_i \exp(\psi_{i-\frac{1}{2}} - \psi_i) =: p_{i-\frac{1}{2}}$$

Since the numerical flux satisfies contact property, we have

$$\hat{\boldsymbol{f}}_{i-\frac{1}{2}} = [0, p_{i-\frac{1}{2}}, 0]^\top, \qquad \hat{\boldsymbol{f}}_{i+\frac{1}{2}} = [0, p_{i+\frac{1}{2}}, 0]^\top$$

The flux in mass and energy equations are zero and the gravitational source term in the energy equation is also zero. Hence the mass and energy equations are already well balanced, i.e.,

$$\frac{\mathrm{d}\boldsymbol{q}^{(1)}_i}{\mathrm{d}t} = 0, \qquad \frac{\mathrm{d}\boldsymbol{q}^{(3)}_i}{\mathrm{d}t} = 0$$

It remains to check the momentum equation. On the left we have

$$\frac{\hat{\boldsymbol{f}}^{(2)}_{i+\frac{1}{2}} - \hat{\boldsymbol{f}}^{(2)}_{i-\frac{1}{2}}}{\Delta x} = \frac{p_{i+\frac{1}{2}} - p_{i-\frac{1}{2}}}{\Delta x}$$

while on the right

$$p_i \mathrm{e}^{-\psi_i} \frac{\mathrm{e}^{\psi_{i+\frac{1}{2}}} - \mathrm{e}^{\psi_{i-\frac{1}{2}}}}{\Delta x} = \frac{p_i \mathrm{e}^{\psi_{i+\frac{1}{2}} - \psi_i} - p_i \mathrm{e}^{\psi_{i-\frac{1}{2}} - \psi_i}}{\Delta x} = \frac{p_{i+\frac{1}{2}} - p_{i-\frac{1}{2}}}{\Delta x}$$

and hence

$$\frac{\mathrm{d}\boldsymbol{q}^{(2)}_i}{\mathrm{d}t} = 0$$

This proves that the initial condition is preserved under any time integration scheme.

REMARK 2. *It is possible to reconstruct density and still retain the result of the previous theorem. In the isothermal case, the quantity* $\rho e^{-\psi}$ *is constant and we can expect the reconstruction of density to be more accurate if we scale the density as in the* $\boldsymbol{w}$ *variables.*

REMARK 3. *For a general temperature profile, the quantities* ψ_i *have to be approximated by quadrature, so that the initial condition in (3.4) is only an approximation to the exact stationary solution. However, by using a special quadrature rule which we explain in next section, we show in Theorem (3) that isothermal and polytropic stationary solutions satisfy equation (3.4) and hence are preserved by the finite volume scheme. A numerical example of a general stationary solution is given in section (4.4).*

3.2. Approximation of source term. Up to this point we have not specified how to approximate $\psi(x)$. The well-balanced property of the scheme as stated in Theorem 1 is independent of the particular appoximation scheme used to compute ψ. In order to preserve isothermal/polytropic solutions exactly, the quadrature rule has to be exact for these cases. To compute the source term in the i'th cell, we define the function $\psi(x)$ as follows

$$\psi(x) = -\int_{x_i}^{x} \frac{\phi'(s)}{RT(s)} \mathrm{d}s$$

where we chose the reference position as x_i. The final scheme will be independent of the choice of this reference position because all the formulae involve only differences in the potential. To approximate the integrals we define the piecewise constant temperature as follows

$$T(x) = \hat{T}_{i+\frac{1}{2}}, \qquad x_i < x < x_{i+1} \tag{3.5}$$

where $\hat{T}_{i+\frac{1}{2}}$ is the logarithmic average given by

$$\hat{T}_{i+\frac{1}{2}} = \frac{T_{i+1} - T_i}{\log T_{i+1} - \log T_i}$$

The integrals are evaluated using the approximation of the temperature given in (3.5) leading to the following expressions for ψ,

$$\begin{aligned}
\psi_i &= 0 \\
\psi_{i-\frac{1}{2}} &= -\frac{1}{R\hat{T}_{i-\frac{1}{2}}} \int_{x_i}^{x_{i-\frac{1}{2}}} \phi'(s)\mathrm{d}s = \frac{\phi_i - \phi_{i-\frac{1}{2}}}{R\hat{T}_{i-\frac{1}{2}}} \\
\psi_{i+\frac{1}{2}} &= -\frac{1}{R\hat{T}_{i+\frac{1}{2}}} \int_{x_i}^{x_{i+\frac{1}{2}}} \phi'(s)\mathrm{d}s = \frac{\phi_i - \phi_{i+\frac{1}{2}}}{R\hat{T}_{i+\frac{1}{2}}}
\end{aligned}$$

The gravitational potential has to be approximated at the cell faces. Since ϕ is obtained from the solution of a Poisson equation it is atleast continuous. Hence we can interpolate the potential from the cell centers to the cell face in a continuous manner. For example the choice

$$\phi_{i+\frac{1}{2}} = \frac{1}{2}(\phi_i + \phi_{i+1})$$

is sufficient to obtain second order accuracy as we show below. Then

$$\psi_{i-\frac{1}{2}} = \frac{\phi_i - \phi_{i-1}}{2R\hat{T}_{i-\frac{1}{2}}}, \qquad \psi_i = 0, \qquad \psi_{i+\frac{1}{2}} = \frac{\phi_i - \phi_{i+1}}{2R\hat{T}_{i+\frac{1}{2}}} \tag{3.6}$$

Note that the above expressions are specific to the i'th cell. Similar expressions must be used for the other cells.

REMARK 4. *The logarithmic average has been used in [5] which also gives a stable method to compute it. We use this stable method to compute the logarithmic average in our numerical implementation.*

THEOREM 3.2. *The source term discretization given by (3.6) is second order accurate.*

Proof: The source term in (3.3) has the factor

$$\mathrm{e}^{-\psi_i} \frac{\mathrm{e}^{\psi_{i+\frac{1}{2}}} - \mathrm{e}^{\psi_{i-\frac{1}{2}}}}{\Delta x} = \frac{\exp\left(\frac{\phi_i - \phi_{i+1}}{2R\hat{T}_{i+\frac{1}{2}}}\right) - \exp\left(\frac{\phi_i - \phi_{i-1}}{2R\hat{T}_{i-\frac{1}{2}}}\right)}{\Delta x} \qquad \text{using (3.6)}$$

Using a Taylor expansion around x_i we get

$$\frac{1}{\hat{T}_{i-\frac{1}{2}}} = \frac{1}{T_i}[1 + O(\Delta x^2)], \qquad \frac{1}{\hat{T}_{i+\frac{1}{2}}} = \frac{1}{T_i}[1 + O(\Delta x^2)] \tag{3.7}$$

Performing a Taylor expansion of the potential around x_i we obtain

$$\begin{aligned}
&\mathrm{e}^{\frac{\phi_i-\phi_{i+1}}{2R\hat{T}_{i+\frac{1}{2}}}} - \mathrm{e}^{\frac{\phi_i-\phi_{i-1}}{2R\hat{T}_{i-\frac{1}{2}}}} \\
&= \mathrm{e}^{\frac{1}{2RT_i}(-\phi_i'\Delta x - \phi_i''\Delta x^2 + O(\Delta x^3))} - \mathrm{e}^{\frac{1}{2RT_i}(+\phi_i'\Delta x - \phi_i''\Delta x^2 + O(\Delta x^3))} \\
&= \left[1 + \frac{1}{2RT_i}(-\phi_i'\Delta x - \phi_i''\Delta x^2) + \frac{1}{2(2RT_i)^2}(\phi_i'\Delta x)^2 + O(\Delta x^3)\right] \\
&\quad - \left[1 + \frac{1}{2RT_i}(\phi_i'\Delta x - \phi_i''\Delta x^2) + \frac{1}{2(2RT_i)^2}(\phi_i'\Delta x)^2 + O(\Delta x^3)\right] \\
&= -\frac{1}{RT_i}\phi'(x_i)\Delta x + O(\Delta x^3)
\end{aligned}$$

Hence the source term discretization is second order accurate.

Remark 5. *The property (3.7) is surprising since we would have only expected first order accuracy. We obtain extra degree of accuracy due to the logarithmic average. If the temperature is discontinuous near some grid point i, then (3.7) is not valid and instead we obtain*

$$\begin{aligned}
&e^{\frac{\phi_i-\phi_{i+1}}{2R\hat{T}_{i+\frac{1}{2}}}} - e^{\frac{\phi_i-\phi_{i-1}}{2R\hat{T}_{i-\frac{1}{2}}}} \\
&= \frac{\phi_i - \phi_{i+1}}{2R\hat{T}_{i+\frac{1}{2}}} - \frac{\phi_i - \phi_{i-1}}{2R\hat{T}_{i-\frac{1}{2}}} + O(\Delta x^2) \\
&= -\left(\frac{1}{2R\hat{T}_{i-\frac{1}{2}}} + \frac{1}{2R\hat{T}_{i+\frac{1}{2}}}\right)\phi_i'\Delta x + O(\Delta x^2)
\end{aligned}$$

Hence the source term discretization has following consistency

$$-p_i\left(\frac{1}{2R\hat{T}_{i-\frac{1}{2}}} + \frac{1}{2R\hat{T}_{i+\frac{1}{2}}}\right)\phi_i' + O(\Delta x)$$

This is not strictly consistent with the exact source term $-\rho_i\frac{\partial\phi}{\partial x}$. In order to study the effect of this, we present 1-D test cases with discontinuous solutions in section (4.6) and (4.7) which are compared with a standard scheme. These results do not show any anamoly in the solutions due to this issue.

Theorem 3.3. *Any hydrostatic solution which is isothermal or polytropic is exactly preserved by the finite volume scheme (3.3).*

Proof: Assume that the initial condition is taken to be a hydrostatic solution. We have to verify that the initial condition satisfies equation (3.4). If the initial condition is isothermal, then $\hat{T}_{i+\frac{1}{2}} = T_e = \text{const}$, and using (2.3) we obtain

$$\frac{p_{i+1}\mathrm{e}^{-\psi_{i+1}}}{p_i\mathrm{e}^{-\psi_i}} = \frac{p_{i+1}}{p_i}\mathrm{e}^{\psi_i-\psi_{i+1}} = \frac{p_{i+1}}{p_i}\exp\left(\frac{\phi_{i+1}-\phi_i}{RT_e}\right) = \frac{p_{i+1}\exp(\phi_{i+1}/RT_e)}{p_i\exp(\phi_i/RT_e)} = 1$$

If the initial condition is polytropic, then

$$\frac{p_{i+1}\mathrm{e}^{-\psi_{i+1}}}{p_i\mathrm{e}^{-\psi_i}} = \frac{p_{i+1}}{p_i}\mathrm{e}^{\psi_i-\psi_{i+1}} = \frac{p_{i+1}}{p_i}\exp\left(\frac{\phi_{i+1}-\phi_i}{R\hat{T}_{i+\frac{1}{2}}}\right)$$

But from (2.4), (2.5) we have

$$\frac{\phi_{i+1}-\phi_i}{R\hat{T}_{i+\frac{1}{2}}} = -\frac{\frac{\nu R}{\nu-1}(T_{i+1}-T_i)}{R\frac{T_{i+1}-T_i}{\log(T_{i+1})-\log(T_i)}} = \log\left(\frac{T_i}{T_{i+1}}\right)^{\frac{\nu}{\nu-1}}$$

and hence

$$\frac{p_{i+1}\mathrm{e}^{-\psi_{i+1}}}{p_i\mathrm{e}^{-\psi_i}} = \frac{p_{i+1}T_{i+1}^{-\nu/(\nu-1)}}{p_iT_i^{-\nu/(\nu-1)}} = 1$$

Hence in both cases, the initial condition is preserved by the finite volume scheme.

3.3. Summary of the scheme. Using the approximations given by (3.6), the semi-discrete finite volume scheme can be written as

$$\frac{\mathrm{d}\boldsymbol{q}_i}{\mathrm{d}t} + \frac{\hat{\boldsymbol{f}}_{i+\frac{1}{2}} - \hat{\boldsymbol{f}}_{i-\frac{1}{2}}}{\Delta x} = \frac{\mathrm{e}^{\hat{\beta}_{i+\frac{1}{2}}(\phi_i-\phi_{i+1})} - \mathrm{e}^{\hat{\beta}_{i-\frac{1}{2}}(\phi_i-\phi_{i-1})}}{\Delta x}\begin{bmatrix}0\\ p_i\\ p_iu_i\end{bmatrix}$$

where we have introduced the quantity

$$\hat{\beta}_{i+\frac{1}{2}} = \frac{1}{2R\hat{T}_{i+\frac{1}{2}}}$$

As an example of reconstruction, we discuss the minmod-type scheme for the interface $i+\frac{1}{2}$. The left and right reconstructed values of the $\boldsymbol{w}$ variables from cells i and $i+1$ respectively are given by

$$\boldsymbol{w}^L_{i+\frac{1}{2}} = \boldsymbol{w}_i + \frac{1}{2}\mathcal{M}(\theta(\boldsymbol{w}_i-\boldsymbol{w}_{i-1}), (\boldsymbol{w}_{i+1}-\boldsymbol{w}_{i-1})/2, \theta(\boldsymbol{w}_{i+1}-\boldsymbol{w}_i))$$

$$\boldsymbol{w}^R_{i+\frac{1}{2}} = \boldsymbol{w}_{i+1} - \frac{1}{2}\mathcal{M}(\theta(\boldsymbol{w}_{i+1}-\boldsymbol{w}_i), (\boldsymbol{w}_{i+2}-\boldsymbol{w}_{i+1})/2, \theta(\boldsymbol{w}_{i+2}-\boldsymbol{w}_{i+1}))$$

where $\theta \in [1,2]$ and $\mathcal{M}(\cdot,\cdot,\cdot)$ is the minmod limiter function which is defined as follows

$$\mathcal{M}(a,b,c) = \begin{cases} s\min(|a|,|b|,|c|) & \text{if } s = \mathrm{sign}(a) = \mathrm{sign}(b) = \mathrm{sign}(c) \\ 0 & \text{otherwise} \end{cases}$$

The variables $\boldsymbol{w}$ are defined using the potential relative to $x_{i+\frac{1}{2}}$. Thus the function ψ is defined by

$$\psi(x) = -\int_{x_{i+\frac{1}{2}}}^{x} \frac{\phi'(s)}{RT(s)}\mathrm{d}s$$

Using the temperature distribution (3.5) and evaluating ψ at the grid points yields

$$\begin{aligned}
\psi_{i-1} &= \frac{\phi_i-\phi_{i-1}}{R\hat{T}_{i-\frac{1}{2}}} + \frac{\phi_{i+\frac{1}{2}}-\phi_i}{R\hat{T}_{i+\frac{1}{2}}} = 2\hat{\beta}_{i-\frac{1}{2}}(\phi_i-\phi_{i-1}) + \hat{\beta}_{i+\frac{1}{2}}(\phi_{i+1}-\phi_i)\\
\psi_i &= \frac{\phi_{i+\frac{1}{2}}-\phi_i}{R\hat{T}_{i+\frac{1}{2}}} = \hat{\beta}_{i+\frac{1}{2}}(\phi_{i+1}-\phi_i)\\
\psi_{i+1} &= -\frac{\phi_{i+1}-\phi_{i+\frac{1}{2}}}{R\hat{T}_{i+\frac{1}{2}}} = -\hat{\beta}_{i+\frac{1}{2}}(\phi_{i+1}-\phi_i)\\
\psi_{i+2} &= -\frac{\phi_{i+1}-\phi_{i+\frac{1}{2}}}{R\hat{T}_{i+\frac{1}{2}}} - \frac{\phi_{i+2}-\phi_{i+1}}{R\hat{T}_{i+\frac{3}{2}}} = -\hat{\beta}_{i+\frac{1}{2}}(\phi_{i+1}-\phi_i) - 2\hat{\beta}_{i+\frac{3}{2}}(\phi_{i+2}-\phi_{i+1})
\end{aligned}$$

	Potential 1	Potential 2	Potential 3
$\phi(x)$	x	$\frac{1}{2}x^2$	$\sin(2\pi x)$

TABLE 1
Potential functions used for well-balanced tests

Potential	Cells	Density	Velocity	Pressure
x	100	8.21676e-15	4.98682e-16	9.19209e-15
	1000	8.00369e-14	1.51719e-14	9.15152e-14
$\frac{1}{2}x^2$	100	1.01874e-14	2.49332e-16	1.06837e-14
	1000	1.05202e-13	4.10434e-16	1.11861e-13
$\sin(2\pi x)$	100	1.12466e-14	5.79978e-16	1.74966e-14
	1000	1.16191e-13	2.93729e-15	1.76361e-13

TABLE 2
Error in density, velocity and pressure for isothermal examples of section (4.1) using potentials from Table (1)

In terms of the above ψ_i's, the variables $\boldsymbol{w}$ are defined as follows

$$\boldsymbol{w}_j = \left[\rho_j \mathrm{e}^{-\psi_j},\ u_j,\ p_j \mathrm{e}^{-\psi_j}\right]^\top, \qquad j = i-1, i, i+1, i+2$$

Once $\boldsymbol{w}^L_{i+\frac{1}{2}}$, $\boldsymbol{w}^R_{i+\frac{1}{2}}$ are computed we obtain the primitive variables by doing an inverse transformation. Since $\psi_{i+\frac{1}{2}} = 0$ we have the following simple relationship

$$\boldsymbol{w}^L_{i+\frac{1}{2}} = \left[\rho^L_{i+\frac{1}{2}},\ u^L_{i+\frac{1}{2}},\ p^L_{i+\frac{1}{2}}\right]^\top \qquad \text{and} \qquad \boldsymbol{w}^R_{i+\frac{1}{2}} = \left[\rho^R_{i+\frac{1}{2}}\ u^R_{i+\frac{1}{2}},\ p^R_{i+\frac{1}{2}}\right]^\top$$

For the first and last cells, we extrapolate the potential from inside the domain to the faces located on the domain boundary

$$\phi_{\frac{1}{2}} = \frac{3}{2}\phi_1 - \frac{1}{2}\phi_2, \qquad \phi_{N+\frac{1}{2}} = \frac{3}{2}\phi_N - \frac{1}{2}\phi_{N-1}$$

4. 1-D numerical results. In all the examples in this section, the domain is the interval $[0, 1]$, the initial condition has zero velocity and the ratio of specific heats is $\gamma = 1.4$. The boundaries are treated as solid walls and time integration is performed using the 3-stage strong stability preserving Runge-Kutta scheme [12]. All the errors reported are measured in L^1 norm and computations are performed in double precision.

4.1. Isothermal examples: well-balanced test. For isothermal equilibrium solutions, we study the well-balanced property for three different potential functions as shown in table (1). The density and pressure are given by

$$\rho_e(x) = p_e(x) = \exp(-\phi(x))$$

The initial condition is taken to be the above hydrostatic solution. The tests are performed on grids with 100 and 1000 cells upto a final time of $t = 2.0$ and the error in density, velocity and pressure are reported in tables (2). We see that the error in the solution is of the order of machine precision. The solutions residuals are also of the order of machine precision.

4.2. Isentropic examples: well-balanced test. In this section we consider isentropic hydrostatic solutions of the form

$$T_e(x) = 1 - \frac{\gamma - 1}{\gamma}\phi(x), \qquad \rho_e = T_e^{\frac{1}{\gamma-1}}, \qquad p_e = \rho_e^\gamma$$

Potential	Cells	Density	Velocity	Pressure
x	100	6.86395e-15	2.65535e-16	7.88869e-15
	1000	7.03820e-14	7.79350e-16	8.03623e-14
$\frac{1}{2}x^2$	100	1.06604e-14	2.27512e-16	1.04128e-14
	1000	1.10726e-13	1.15415e-15	1.09185e-13
$\sin(2\pi x)$	100	1.27570e-14	5.18212e-16	1.65185e-14
	1000	1.29020e-13	1.12837e-15	1.66566e-13

TABLE 3
Error in density, velocity and pressure for isentropic examples of section (4.2) using potentials from Table (1)

Potential	Cells	Density	Velocity	Pressure
x	100	6.86395e-15	2.65535e-16	7.88869e-15
	1000	7.03820e-14	7.79350e-16	8.03623e-14
$\frac{1}{2}x^2$	100	1.06604e-14	2.27512e-16	1.04128e-14
	1000	1.10726e-13	1.15415e-15	1.09185e-13
$\sin(2\pi x)$	100	1.27570e-14	5.18212e-16	1.65185e-14
	1000	1.29020e-13	1.12837e-15	1.66566e-13

TABLE 4
Error in density, velocity and pressure for polytropic examples of section (4.2) using potentials from Table (1)

We take the initial condition to be the above hydrostatic solution and apply the scheme on a grid with 100 and 1000 cells upto a final time of $t = 2.0$ and the error in density, velocity and pressure are reported in tables (3). We see that the error in the solution is of the order of machine precision. The solutions residuals are also of the order of machine precision.

4.3. Polytropic examples: well-balanced test. In this section we consider polytropic hydrostatic solutions of the form

$$T_e(x) = 1 - \frac{\nu - 1}{\nu}\phi(x), \qquad \rho_e = T_e^{\frac{1}{\nu-1}}, \qquad p_e = \rho_e^{\nu}$$

with ν different from γ; we take $\nu = 1.2$ in the tests. We take the initial condition to be the above hydrostatic solution and apply the scheme on a grid with 100 and 1000 cells upto a final time of $t = 2.0$ and the error in density, velocity and pressure are reported in tables (4). We see that the error in the solution is of the order of machine precision. The solutions residuals are also of the order of machine precision.

4.4. Non-isothermal example. The stationary solution is given by the following

$$\phi(x) = \frac{1}{2}x^2, \qquad \rho_e(x) = \exp(-x), \qquad p_e(x) = (1+x)\exp(-x)$$

which corresponds to a non-uniform temperature profile given by $T_e(x) = 1 + x$. This solution is neither isothermal nor polytropic and the present scheme will not be able to preserve the exact hydrostatic solution. Instead, we construct an approximation to the above hydrostatic solution by numerically integrating the hydrostatic equations (2.2) as follows.

$$p_1 = p_e(x_1), \qquad \rho_1 = \frac{p_1}{RT_e(x_1)}$$

$$p_i = p_{i-1}\exp(-2\hat{\beta}_{i-\frac{1}{2}}(\phi_i - \phi_{i-1})), \qquad \rho_i = \frac{p_i}{RT_e(x_i)}, \qquad i = 2, 3, \ldots, N$$

Cells	ρ error	ρ rate	Velocity	p error	p rate
50	5.41510e-06	-	3.90665e-16	8.51248e-06	
100	1.37964e-06	1.97	1.06754e-15	2.16486e-06	1.97
200	3.48173e-07	1.98	4.82755e-16	5.45846e-07	1.98
400	8.74530e-08	1.99	1.94554e-15	1.37043e-07	1.99
800	2.19146e-08	1.99	2.62298e-15	3.43336e-08	1.99
1600	5.48521e-09	1.99	6.56911e-15	8.59273e-09	1.99

TABLE 5
Convergence of error for hydrostatic solution of section (4.4).

The above solution satisfies equation (3.4) and hence is preserved by the numerical scheme. If we apply the finite volume scheme to the above discrete solution, then the residuals are of the order of machine precision and the initial condition is preserved. We compute the solution upto a time of $t = 2$ and then measure the error in the numerical solution relative to the exact hydrostatic solution on different grid sizes. The errors and convergence rates shown in table (5) indicate a second order accuracy. The velocity is zero upto machine precision indicating that we have a stationary solution.

4.5. Evolution of small perturbations. In this example we study the evolution of a small perturbation added to the initial isothermal hydrostatic solution which is similar to the test case in [9]. The initial condition is taken to be the following

$$\phi = \frac{1}{2}x^2, \quad u = 0, \quad \rho(x) = \exp(-\phi(x)), \quad p(x) = \exp(-\phi(x)) + \varepsilon \exp(-100(x - 1/2)^2)$$

where the amplitude ε in the pressure perturbation will be varied. Figure (1) shows the results using our well-balanced scheme and a non-well-balanced scheme in which the source term is discretized with central differences

$$\frac{\partial \phi}{\partial x}(x_i) \approx \frac{\phi_{i+1} - \phi_{i-1}}{2\Delta x}$$

and we reconstruct the primitive variables ρ, u, p. For a large perturbation of $\varepsilon = 10^{-3}$, figure (1a) shows that the non-well-balanced scheme also gives good solutions on 100 cells. But for a smaller perturbation of $\varepsilon = 10^{-5}$, figure (1b) shows that the non-well-balanced scheme performs poorly on 100 cells. With 500 cells, the non-well-balanced scheme also shows similar results as the well-balanced scheme, see figure (1c). This clearly shows that improved accuracy is obtained with a well-balanced scheme on coarser meshes which cannot be achieved with other non-well-balanced schemes. In figure (1d) we compare the solutions from 100 and 500 cells of the well-balanced schemes to shows that the solutions are very accurate even on the coarser mesh.

4.6. Shock tube under gravitational field. We consider the standard Sod test case together with a gravitational field $\phi(x) = x$ as in [15]. The domain is $[0, 1]$ and the initial conditions are given by

$$(\rho, u, p) = \begin{cases} (1, 0, 1) & x < \frac{1}{2} \\ (0.125, 0, 0.1) & x > \frac{1}{2} \end{cases}$$

together with solid wall boundary conditions. The solutions are obtained on 100 and 2000 cells until a time of $t = 0.2$ and are shown in figures (2). We see that the density increases near $x = 0$ due to the gravitational force which is directed to the left. The coarse mesh of 100 cells is already

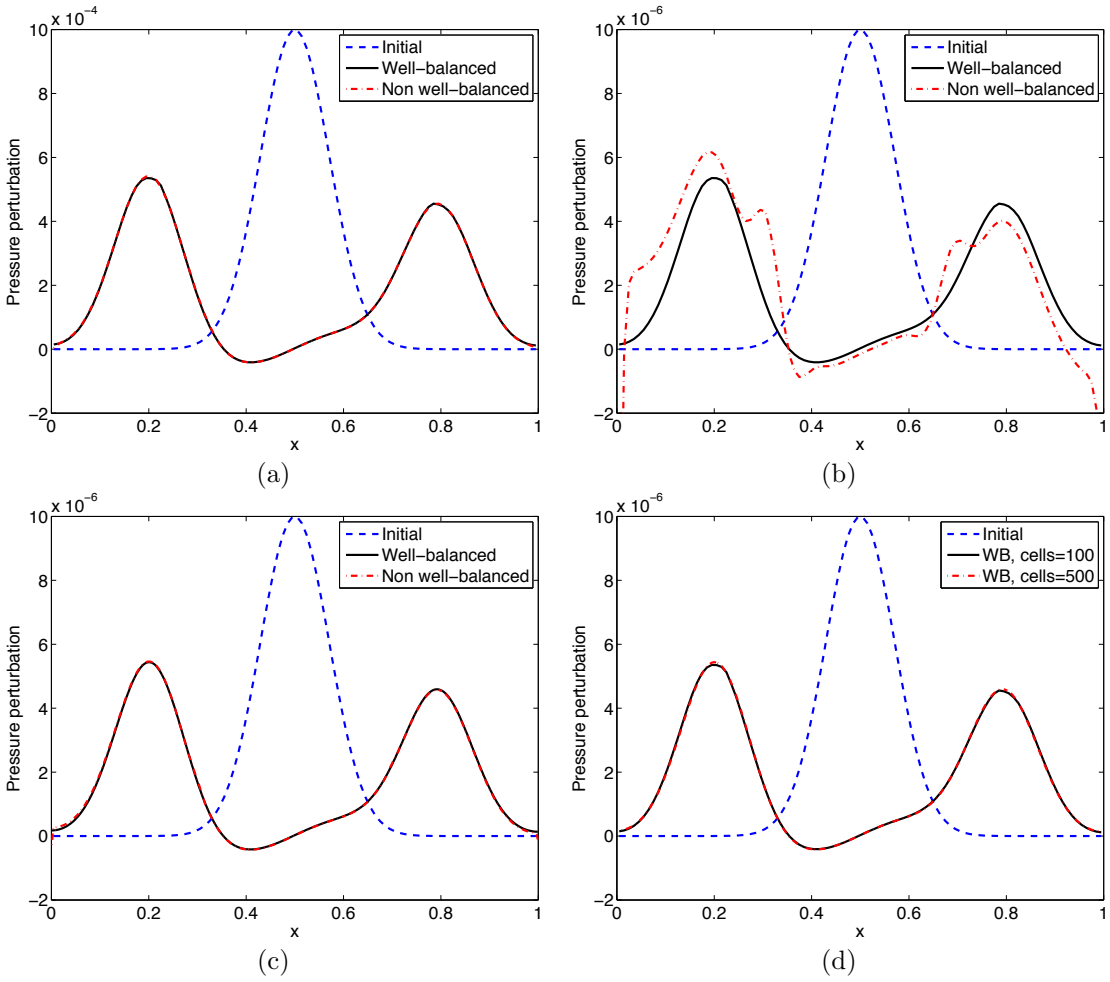

FIG. 1. *Evolution of pressure perturbations: (a) $\varepsilon = 10^{-3}$, 100 cells, (b) $\varepsilon = 10^{-5}$, 100 cells, (c) $\varepsilon = 10^{-5}$, 500 cells, (d) $\varepsilon = 10^{-5}$*

able to resolve all the features in the solution and there are no spurious oscillations. This test indicates that the modifications in reconstruction scheme and source term are not destroying the non-oscillatory nature of the scheme.

4.7. Contact discontinuity under gravitational field. In this test case, we consider an initial contact discontinuity under a gravitational field $\phi(x) = x$. The domain is $[0, 1]$ and the initial conditions are given by

$$(\rho, u, p) = \begin{cases} (1, 0, 1) & x < \frac{1}{2} \\ (10, 0, 1) & x > \frac{1}{2} \end{cases}$$

together with solid wall boundary conditions at both ends. We take $\gamma = 1.4$ and the solution is computed upto a time of $t = 0.6$. In figure (3), we show the results obtained with our well-balanced scheme and a standard finite volume scheme in which the source terms are added in their standard form (see equation (2.1)) with reconstruction of primitive variables. The

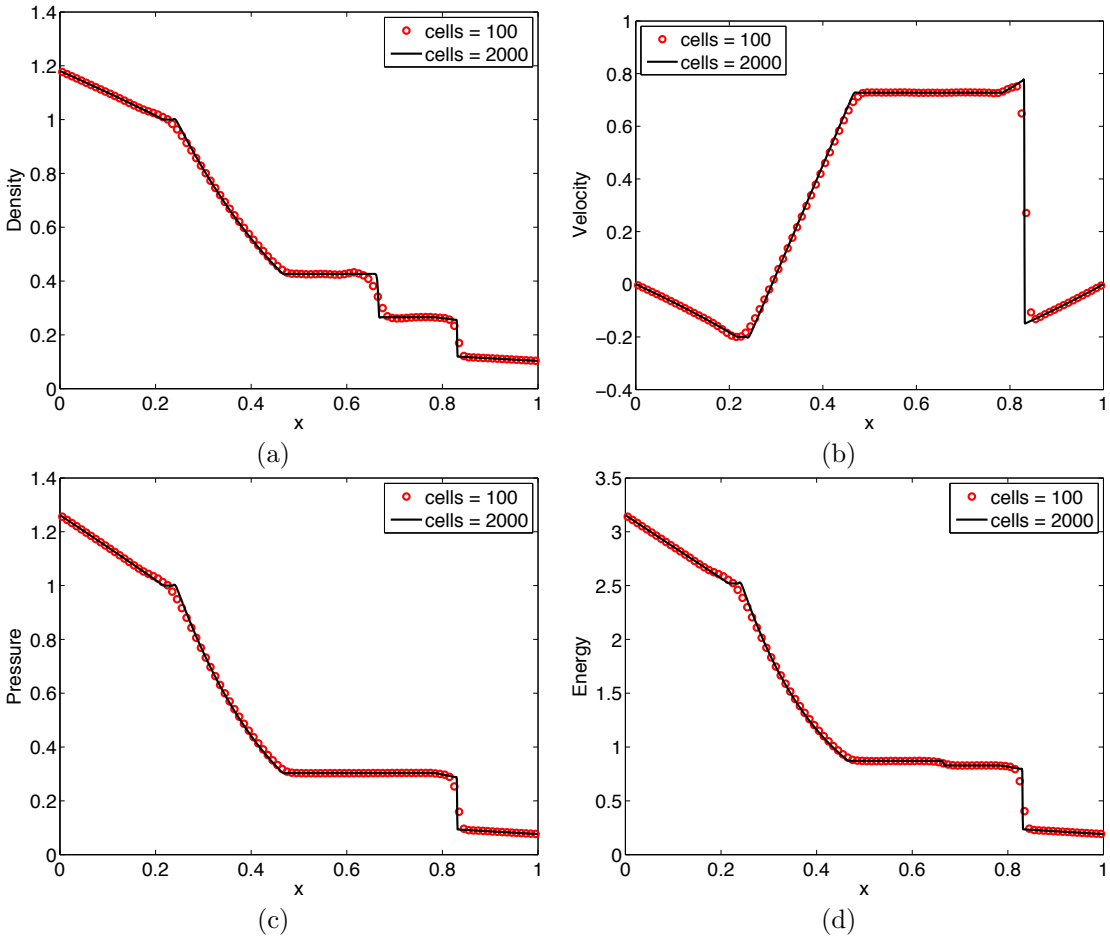

FIG. 2. *Sod test under gravitational field at time* $t = 0.2$. *(a) Density, (b) Velocity, (c) Pressure, (d) Energy*

solutions are computed on meshes with 200 and 2000 cells and we observe that both schemes give similar results. The large temperature jump does not cause any abnormalities in the solution computed with the well-balanced scheme, even though the source term discretization is not formally consistent in this case.

5. 2-D Euler equations with gravity. The 2-D Euler equations in Cartesian coordinates is a system of four conservation laws for mass, momentum and energy, which can be written as

$$\frac{\partial \boldsymbol{q}}{\partial t} + \frac{\partial \boldsymbol{f}}{\partial x} + \frac{\partial \boldsymbol{g}}{\partial y} = \boldsymbol{s}$$

Here the conserved variables $\boldsymbol{q}$, fluxes $(\boldsymbol{f}, \boldsymbol{g})$ and source terms $\boldsymbol{s}$ are given by

$$\boldsymbol{q} = \begin{bmatrix} \rho \\ \rho u \\ \rho v \\ E \end{bmatrix}, \quad \boldsymbol{f} = \begin{bmatrix} \rho u \\ p + \rho u^2 \\ \rho uv \\ (E+p)u \end{bmatrix}, \quad \boldsymbol{g} = \begin{bmatrix} \rho v \\ \rho uv \\ p + \rho v^2 \\ (E+p)v \end{bmatrix}, \quad \boldsymbol{s} = \begin{bmatrix} 0 \\ -\rho \frac{\partial \phi}{\partial x} \\ -\rho \frac{\partial \phi}{\partial y} \\ -\rho(u \frac{\partial \phi}{\partial x} + v \frac{\partial \phi}{\partial y}) \end{bmatrix}$$

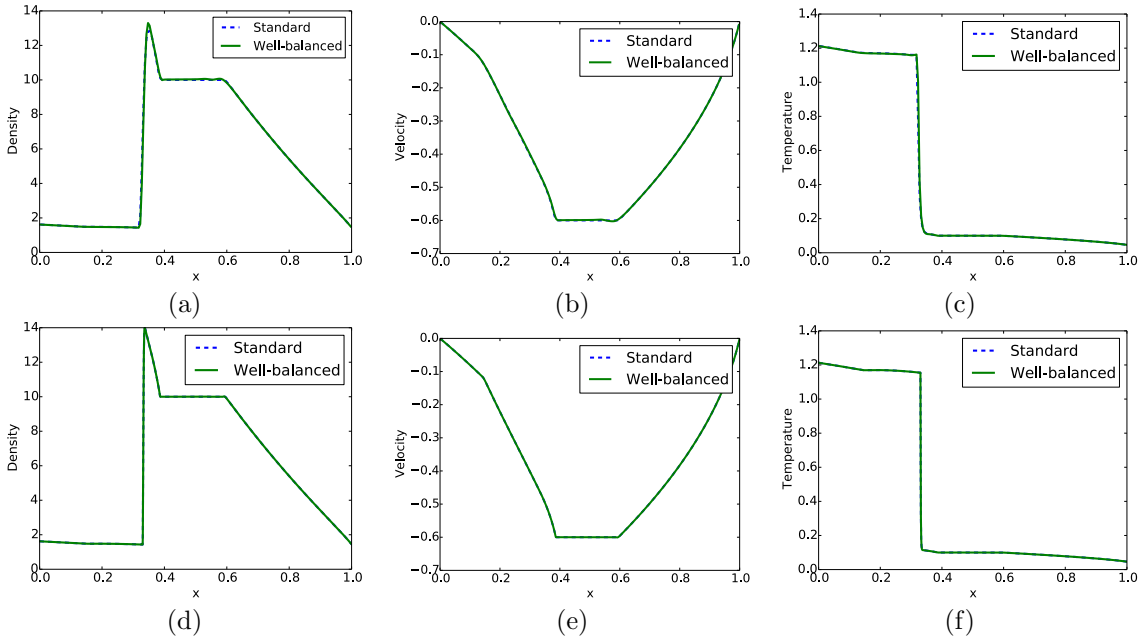

FIG. 3. *1-D contact test case at $t = 0.6$. First row shows solution with 200 cells and second row shows solution with 2000 cells*

In the above equations ρ is the density, (u, v) are the Cartesian components of the velocity, p is the pressure, E is the total energy per unit volume and ϕ is the gravitational potential. In general we consider the potential ϕ to be a function of both spatial coordinates.

5.1. Hydrostatic solution. The hydrostatic equilibrium is characterized by the following set of equations

$$u_e = v_e = 0, \qquad \frac{\partial p_e}{\partial x} = -\rho_e \frac{\partial \phi}{\partial x}, \qquad \frac{\partial p_e}{\partial y} = -\rho_e \frac{\partial \phi}{\partial y}$$

These equations can be integrated along $y = \text{const}$ and $x = \text{const}$ lines respectively to obtain

$$p_e(x, y) = a(y) \exp\left(- \int_{x_0}^{x} \frac{\phi_x(s, y)}{RT(s, y)} \mathrm{d}s \right), \qquad p_e(x, y) = b(x) \exp\left(- \int_{y_0}^{y} \frac{\phi_y(x, s)}{RT(x, s)} \mathrm{d}s \right)$$

As in the 1-D case, we will exploit the structure of these solutions to construct the well-balanced scheme.

6. 2-d finite volume scheme on Cartesian meshes. Define

$$\psi(x, y) = - \int_{x_0}^{x} \frac{\phi_x(s, y)}{RT(s, y)} \mathrm{d}s, \qquad \chi(x, y) = - \int_{y_0}^{y} \frac{\phi_y(x, s)}{RT(x, s)} \mathrm{d}s$$

Then the gravitational force can be written as

$$-\rho \phi_x = p \mathrm{e}^{-\psi} \frac{\partial}{\partial x} \mathrm{e}^{\psi}, \qquad -\rho \phi_y = p \mathrm{e}^{-\chi} \frac{\partial}{\partial y} \mathrm{e}^{\chi} \tag{6.1}$$

Consider a partition of the computational domain into rectangular cells defined by $(x_{i-\frac{1}{2}}, x_{i+\frac{1}{2}}) \times (y_{j-\frac{1}{2}}, y_{j+\frac{1}{2}})$ with $x_{i+\frac{1}{2}} - x_{i-\frac{1}{2}} = \Delta x$ and $y_{j+\frac{1}{2}} - y_{j-\frac{1}{2}} = \Delta y$. The cells are indexed by the tuple

(i,j). As in the 1-D case, we approximate the source terms in the form given by equation (6.1) by using a finite difference scheme leading to the following semi-discrete finite volume scheme for the cell (i,j)

$$\Omega_{i,j}\frac{\mathrm{d}}{\mathrm{d}t}\boldsymbol{q}_{i,j} + \hat{\boldsymbol{f}}_{i+\frac{1}{2},j} - \hat{\boldsymbol{f}}_{i-\frac{1}{2},j} + \hat{\boldsymbol{g}}_{i,j+\frac{1}{2}} - \hat{\boldsymbol{g}}_{i,j-\frac{1}{2}} = \hat{\boldsymbol{s}}_{i,j} \tag{6.2}$$

The gravitational source term is discretized as

$$\begin{aligned}
\hat{\boldsymbol{s}}^{(1)}_{i,j} &= 0 \\
\hat{\boldsymbol{s}}^{(2)}_{i,j} &= p_{i,j}\mathrm{e}^{-\psi_{i,j}}\left[\mathrm{e}^{\psi_{i+\frac{1}{2},j}} - \mathrm{e}^{\psi_{i-\frac{1}{2},j}}\right] \\
\hat{\boldsymbol{s}}^{(3)}_{i,j} &= p_{i,j}\mathrm{e}^{-\chi_{i,j}}\left[\mathrm{e}^{\chi_{i,j+\frac{1}{2}}} - \mathrm{e}^{\chi_{i,j-\frac{1}{2}}}\right] \\
\hat{\boldsymbol{s}}^{(4)}_{i,j} &= u_{i,j}\hat{\boldsymbol{s}}^{(2)}_{i,j} + v_{i,j}\hat{\boldsymbol{s}}^{(3)}_{i,j}
\end{aligned}$$

Following the steps in the 1-D case, we can write the source terms as

$$\begin{aligned}
\hat{\boldsymbol{s}}^{(2)}_{i,j} &= p_{i,j}\left[\mathrm{e}^{\hat{\beta}_{i+\frac{1}{2},j}(\phi_{i+1,j}-\phi_{i,j})} - \mathrm{e}^{\hat{\beta}_{i-\frac{1}{2},j}(\phi_{i-1,j}-\phi_{i,j})}\right] \\
\hat{\boldsymbol{s}}^{(3)}_{i,j} &= p_{i,j}\left[\mathrm{e}^{\hat{\beta}_{i,j+\frac{1}{2}}(\phi_{i,j+1}-\phi_{i,j})} - \mathrm{e}^{\hat{\beta}_{i,j-\frac{1}{2}}(\phi_{i,j-1}-\phi_{i,j})}\right]
\end{aligned}$$

To obtain the values at the face $\boldsymbol{q}^L_{i+\frac{1}{2},j}$, $\boldsymbol{q}^R_{i+\frac{1}{2},j}$ we reconstruct the following set of variables

$$\boldsymbol{w} = [\rho\mathrm{e}^{-\psi}, u, v, p\mathrm{e}^{-\psi}]^\top$$

and to obtain $\boldsymbol{q}^L_{i,j+\frac{1}{2}}$, $\boldsymbol{q}^R_{i,j+\frac{1}{2}}$, we reconstruct the following set of variables

$$\boldsymbol{w} = [\rho\mathrm{e}^{-\chi}, u, v, p\mathrm{e}^{-\chi}]^\top$$

The detailed equations are similar to the 1-D equations given in section (3.3) but applied dimension by dimension. We next state without proof, the theorems related to well-balanced property and preservation of isothermal and polytropic solutions. The proofs are similar to the 1-D case and hence we do not repeat them. The pressure forces along each coordinate direction are balanced by the gravitational force in the same direction, just as in the 1-D case.

THEOREM 6.1. *The finite volume scheme (6.2) together with a numerical flux which satisfies* contact property *and reconstruction of* $\boldsymbol{w}$ *variables is well-balanced in the sense that the initial condition given by*

$$u_{i,j} = v_{i,j} = 0, \qquad p_{i,j}\exp(-\psi_{i,j}) = a_j, \qquad p_{i,j}\exp(-\chi_{i,j}) = b_i, \qquad \forall\ i,j \tag{6.3}$$

is preserved by the numerical scheme.

THEOREM 6.2. *Any hydrostatic solution which is isothermal or polytropic is exactly preserved by the finite volume scheme (6.2).*

7. 2-D numerical results. In all the test cases, we consider an ideal gas with $\gamma = 1.4$. The time integration is performed by the 3-stage strong stability preserving Runge-Kutta scheme [12]. All computations are performed in double precision.

Grid	ρ	u	v	p
50×50	0.19050E-14	0.14660E-15	0.14439E-15	0.20428E-14
200×200	0.75677E-14	0.12908E-14	0.12853E-14	0.83936E-14

TABLE 6
Error in density, velocity and pressure for isothermal hydrostatic example of section (7.1).

Grid	ρ	u	v	p
50×50	0.20449E-14	0.41148E-15	0.39802E-15	0.24637E-14
200×200	0.83747E-14	0.18037E-14	0.17986E-14	0.10107E-13

TABLE 7
Error in density, velocity and pressure for polytropic hydrostatic example of section (7.2).

7.1. Isothermal hydrostatic solution. Consider the isothermal hydrostatic solution in the unit square corresponding to the potential $\phi(x, y) = x + y$ given by

$$\rho_e(x, y) = \rho_0 \exp(-\rho_0 g(x + y)/p_0), \qquad p_e(x, y) = p_0 \exp(-\rho_0 g(x + y)/p_0)$$

Following [15], we take the parameters to be $\rho_0 = 1.21$, $p_0 = 1$ and $g = 1$. We first perform a test of well-balanced property by starting the computations with hydrostatic solution as initial condition and solve upto a time of $t = 1$. The error in the solution with respect to the hydrostatic solution is shown in table (6) for two different grid sizes. We note that these errors are of the order of machine precision which shows the well-balanced property of the scheme.

To study the accuracy of the scheme, we add an initial perturbation to the pressure and take the following initial condition

$$p(x, y, 0) = p_0 \exp(-\rho_0 g(x + y)/p_0) + \eta \exp(-100\rho_0 g((x - 0.3)^2 + (y - 0.3)^2)/p_0)$$

with the other quantities being same as in the above hydrostatic case. This initial condition is evolved upto a time of $t = 0.15$ with transmissive boundary conditions on a mesh of 50×50 cells using the present well-balanced scheme and a non-well-balanced scheme in which the source terms are discretized with central differences. In figure (4) we show the results for the case of large perturbation with $\eta = 0.1$. The non-well-balanced scheme generates some distortion near the origin which is not seen in the well-balanced results. In figure (5) we show the results for the smaller perturbation of $\eta = 0.001$. The well-balanced scheme is still able to resolve the pressure pulse while there are very large changes observed in the case of the non-well-balanced scheme and the initial pressure pulse is completely destroyed. This test clearly demonstrates the improved accuracy obtained with the well-balanced scheme in resolving small perturbations around the hydrostatic solution.

7.2. Polytropic hydrostatic solution. Consider the polytropic hydrostatic solution in the unit square corresponding to the potential $\phi(x, y) = x + y$ given by

$$\phi = x + y, \qquad T_e = 1 - \frac{\nu - 1}{\nu}(x + y), \qquad p_e = T_e^{\frac{\nu}{\nu-1}}, \qquad \rho_e = T_e^{\frac{1}{\nu-1}}$$

We perform well-balanced test for above solution taking $\nu = 1.2$ and grid sizes of 50×50 and 200×200. The error in solution at time $t = 1$ is reported in table (7) which shows that the solution is preserved upto machine precision.

Next, we consider a perturbation of the initial pressure from the above polytropic solution given by

$$p(x, y, 0) = p_e(x, y) + \eta \exp(-100\rho_0 g((x - 0.3)^2 + (y - 0.3)^2)/p_0)$$

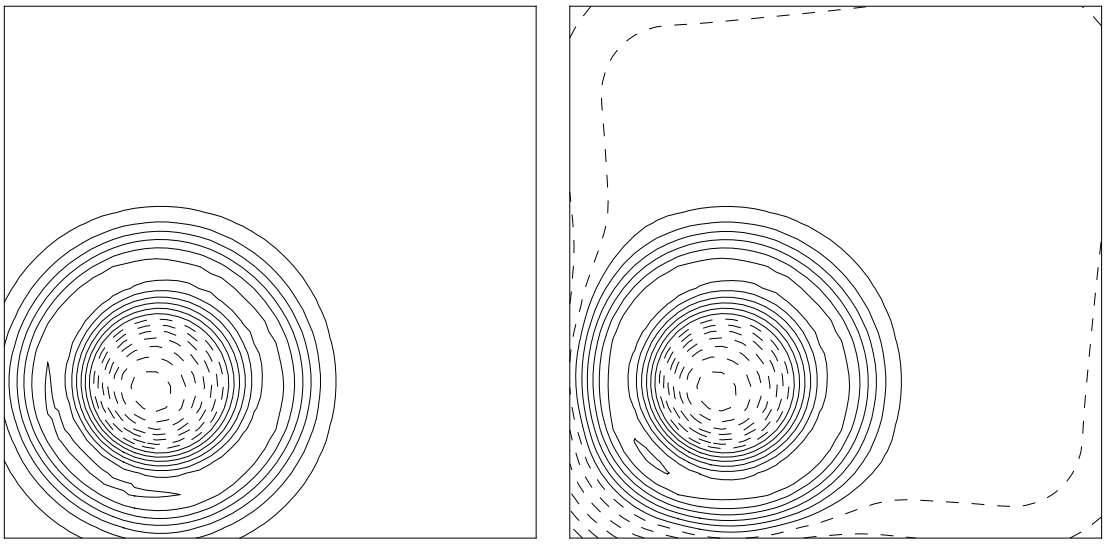

(a) (b)

FIG. 4. *Evolution of pressure perturbation in test case of section (7.1) with $\eta = 0.1$. 20 equally spaced contours between -0.03 and +0.03 are shown. (a) Well-balanced scheme (b) non-well-balanced scheme*

where the parameters in the perturbation are same as in the previous section. This initial condition is evolved upto a time of $t = 0.15$ with transmissive boundary conditions on a mesh of 50×50 cells using the present well-balanced scheme and a non-well-balanced scheme in which the source terms are discretized with central differences. In figure (6) we show the results for the case of large perturbation with $\eta = 0.1$. The non-well-balanced scheme generates some distortion near the origin which is not seen in the well-balanced results. In figure (7) we show the results for the smaller perturbation of $\eta = 0.001$. The well-balanced scheme is still able to show the pressure pulse while there are very large changes observed in the case of the non-well-balanced scheme and the initial pressure pulse is completely destroyed. This test again clearly demonstrates the improved accuracy obtained with the well-balanced scheme in resolving small perturbation around the hydrostatic solution.

7.3. Rayleigh-Taylor instability. In this example, we put a perturbation in density over an isothermal radial solution with potential $\phi = r$. The initial pressure and density are given by

$$p = \begin{cases} \mathrm{e}^{-r} & r \le r_0 \\ \mathrm{e}^{-\frac{r}{\alpha} + r_0 \frac{(1-\alpha)}{\alpha}} & r > r_0 \end{cases}, \qquad \rho = \begin{cases} \mathrm{e}^{-r} & r \le r_i \\ \frac{1}{\alpha}\mathrm{e}^{-\frac{r}{\alpha} + r_0 \frac{(1-\alpha)}{\alpha}} & r > r_i \end{cases}$$

where $r_i = r_0(1 + \eta\cos(k\theta))$ and $\alpha = \exp(-r_0)/(\exp(-r_0) + \Delta_\rho)$. Hence the density jumps by an amount $\Delta_\rho > 0$ at the interface defined by $r = r_i$ whereas the pressure is continuous. Following [9], we take $\Delta_\rho = 0.1$, $\eta = 0.02$, $k = 20$ and use a mesh of 240×240 cells on the domain $[-1, +1] \times [-1, +1]$. In the regions $r < r_0(1-\eta)$ and $r > r_0(1+\eta)$ the initial condition is in stable equilibrium but due to the discontinuous density, a Rayleigh-Taylor instability develops at the interface defined by $r = r_i$. Plots of density at different times are shown in figure (8). We see that the instability is concentrated only around the discontinuous interface which is a consequence of the well-balanced property. If we use a non-well-balanced scheme, then large disturbances develop away from the density interface leading to completely erroneous solution. We do not obtain a radially symmetric solution because our initial condition is not symmetric due

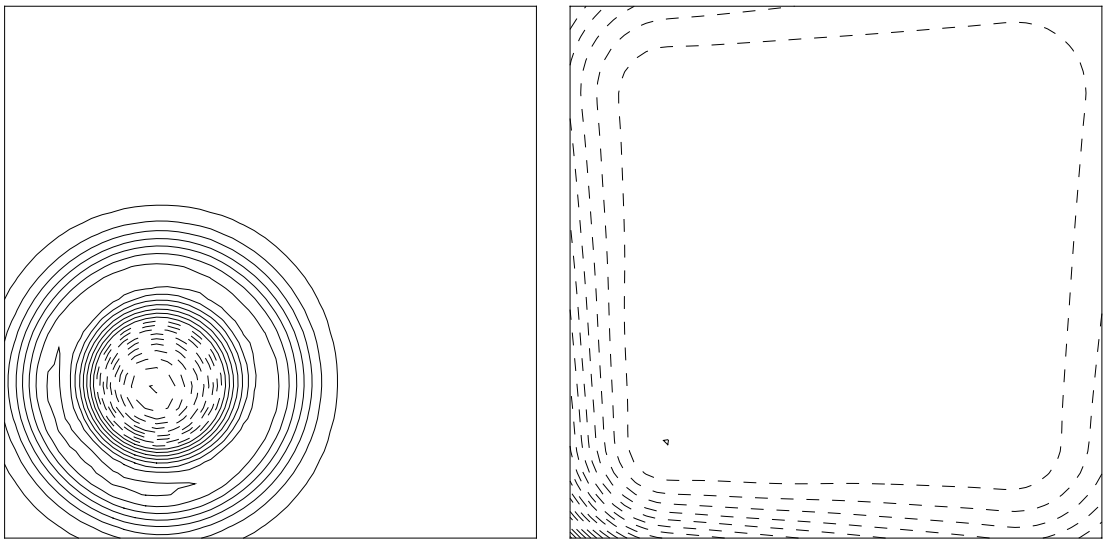

(a) (b)

FIG. 5. *Evolution of pressure perturbation in test case of section (7.1) with* $\eta = 0.001$. *(a) Well-balanced scheme, 20 equally spaced contours between -0.00026 and +0.00026 are shown. (b) non-well-balanced scheme, 20 equally spaced contours between -0.02 and +0.00026 are shown.*

to the use of Cartesian meshes. This test case again shows the advantage of using a well-balanced scheme for flows close to the stationary solution.

8. Summary and conclusions. We construct a novel well-balanced second order finite volume scheme for Euler equations with gravity under the ideal gas assumption. We achieve well-balanced property for isothermal and polytropic hydrostatic solutions with a single scheme. The scheme requires the knowledge of the gravitational potential at the grid points only. The numerical results in one and two dimensions demonstrate the well-balanced property of the scheme and the resulting improved accuracy in resolving small perturbations around the hydrostatic solution. The proposed scheme is a simple modification of the reconstruction step in finite volume schemes and source term discretization which can be easily implemented in existing codes with minimal work. In practical applications like star simulation, it may be necessary to use curvilinear meshes and the present well-balanced scheme has been extended to this case which will be presented elsewhere. Moreover in many astrophysical applications, the Mach number can be very low, necessitating the use of a low-Mach preconditioned scheme [4], e.g., based on the classical Roe scheme. The well-balanced property of the proposed scheme is valid in such cases also. Finally, it is possible to extend the current approach to the case of general equation of state or even tabulated EOS.

Acknowledgments. The first author was supported by the AIRBUS Group Corporate Foundation Chair in Mathematics of Complex Systems established in TIFR/ICTS, Bangalore to visit University of Würzburg for carrying out this work. We acknowledge DAAD for granting a research stay funding (Codenumber: A/13/05198) to visit Univ. of Würzburg during 2013 when this work was initiated. We thank Fritz Röpke and Philipp Edelmann, University of Würzburg, for bringing this problem to our attention in the context of astrophysical flow simulations.

REFERENCES

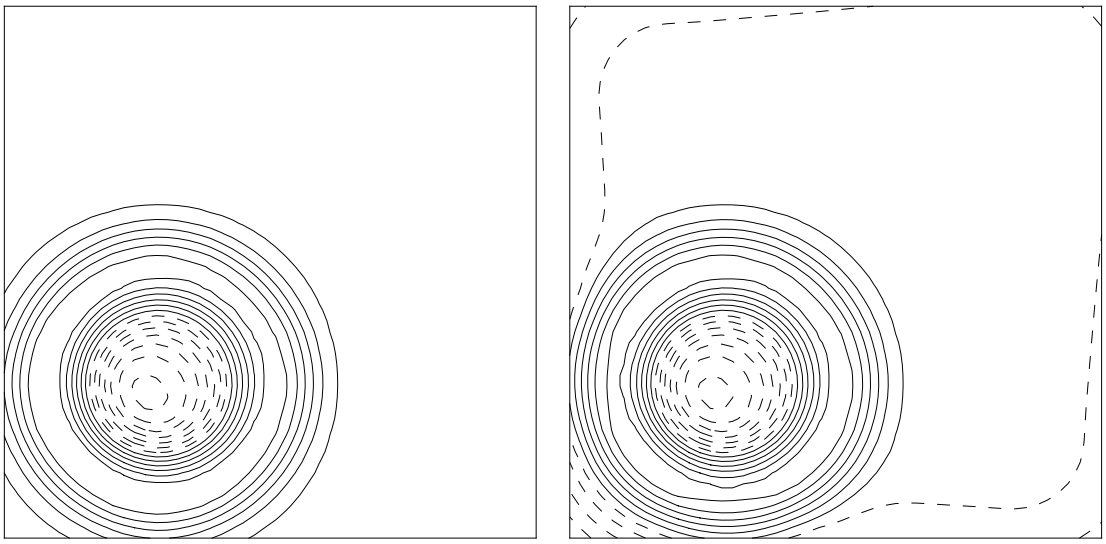

FIG. 6. *Evolution of pressure perturbation in test case of section (7.2) with $\eta = 0.1$. 20 equally spaced contours between -0.03 and +0.03 are shown. (a) Well-balanced scheme, (b) non-well-balanced scheme*

[1] C. BERTHON, V. DESVEAUX, C. KLINGENBERG, AND M. ZENK, *Well balanced schemes to capture non-explicit steady states. Part 2: Euler with gravity*, submitted.

[2] ———, *A well-balanced scheme for the Euler equation with a gravitational potential*, in Proceedings of the Seventh International Symposium on Finite Volumes for Complex Applications, 2014.

[3] F. G. FUCHS, A. D. MCMURRY, S. MISHRA, N. H. RISEBRO, AND K. WAAGAN, *High order well-balanced finite volume schemes for simulating wave propagation in stratified magnetic atmospheres*, J. Comput. Phys., 229 (2010), pp. 4033–4058.

[4] HERVÉ GUILLARD AND CÉCILE VIOZAT, *On the behaviour of upwind schemes in the low mach number limit*, Computers and Fluids, 28 (1999), pp. 63 – 86.

[5] FARZAD ISMAIL AND PHILIP L. ROE, *Affordable, entropy-consistent Euler flux functions II: Entropy production at shocks*, J. Comput. Phys., 228 (2009), pp. 5410–5436.

[6] R. KÄPPELI AND S. MISHRA, *Well-balanced schemes for the Euler equations with gravitation*, J. Comput. Phys., 259 (2014), pp. 199–219.

[7] L. D. LANDAU AND E. M. LIFSCHITZ, *Fluid Mechanics*, Course of Theoretical Physics, Butterworth-Heinemann, 2 ed., 1987.

[8] RANDALL J. LEVEQUE, *A well-balanced path-integral f-wave method for hyperbolic problems with source terms*, J. Sci. Comput., 48 (2011), pp. 209–226.

[9] RANDALL. J. LEVEQUE AND DEREK. S. BALE, *Wave propagation methods for conservation laws with source terms*, in Hyperbolic Problems: Theory, Numerics, Applications, Rolf Jeltsch and Michael Fey, eds., vol. 130 of International Series of Numerical Mathematics, Birkhäuser Basel, 1999, pp. 609–618.

[10] J. LUO, K. XU, AND N. LIU, *A well-balanced symplecticity-preserving gas-kinetic scheme for hydrodynamic equations under gravitational field*, SIAM Journal on Scientific Computing, 33 (2011), pp. 2356–2381.

[11] P. L. ROE, *Approximate Riemann solvers, parameter vectors, and difference schemes*, Journal of Computational Physics, 43 (1981), pp. 357 – 372.

[12] CHI-WANG SHU AND STANLEY OSHER, *Efficient implementation of essentially non-oscillatory shock-capturing schemes*, Journal of Computational Physics, 77 (1988), pp. 439 – 471.

[13] E.F. TORO, M. SPRUCE, AND W. SPEARES, *Restoration of the contact surface in the HLL-Riemann solver*, Shock Waves, 4 (1994), pp. 25–34.

[14] R. TOUMA, U. KOLEY, AND C. KLINGENBERG, *Well-balanced unstaggered central scheme for the Euler equation with gravity*, Submitted.

[15] YULONG XING AND CHI-WANG SHU, *High order well-balanced WENO scheme for the gas dynamics equations under gravitational fields*, J. Sci. Comput., 54 (2013), pp. 645–662.

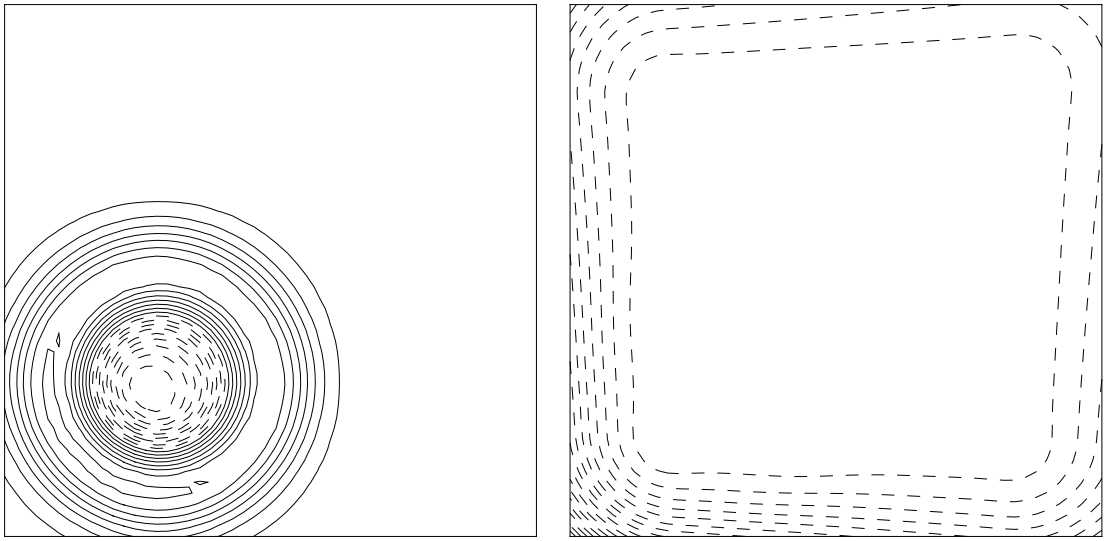

FIG. 7. *Evolution of pressure perturbation in test case of section (7.2) with* $\eta = 0.001$. *(a) Well-balanced scheme, 20 equally spaced contours between -0.00025 and +0.00025 are shown. (b) non-well-balanced scheme, 20 equally spaced contours between -0.015 and +0.0003 are shown.*

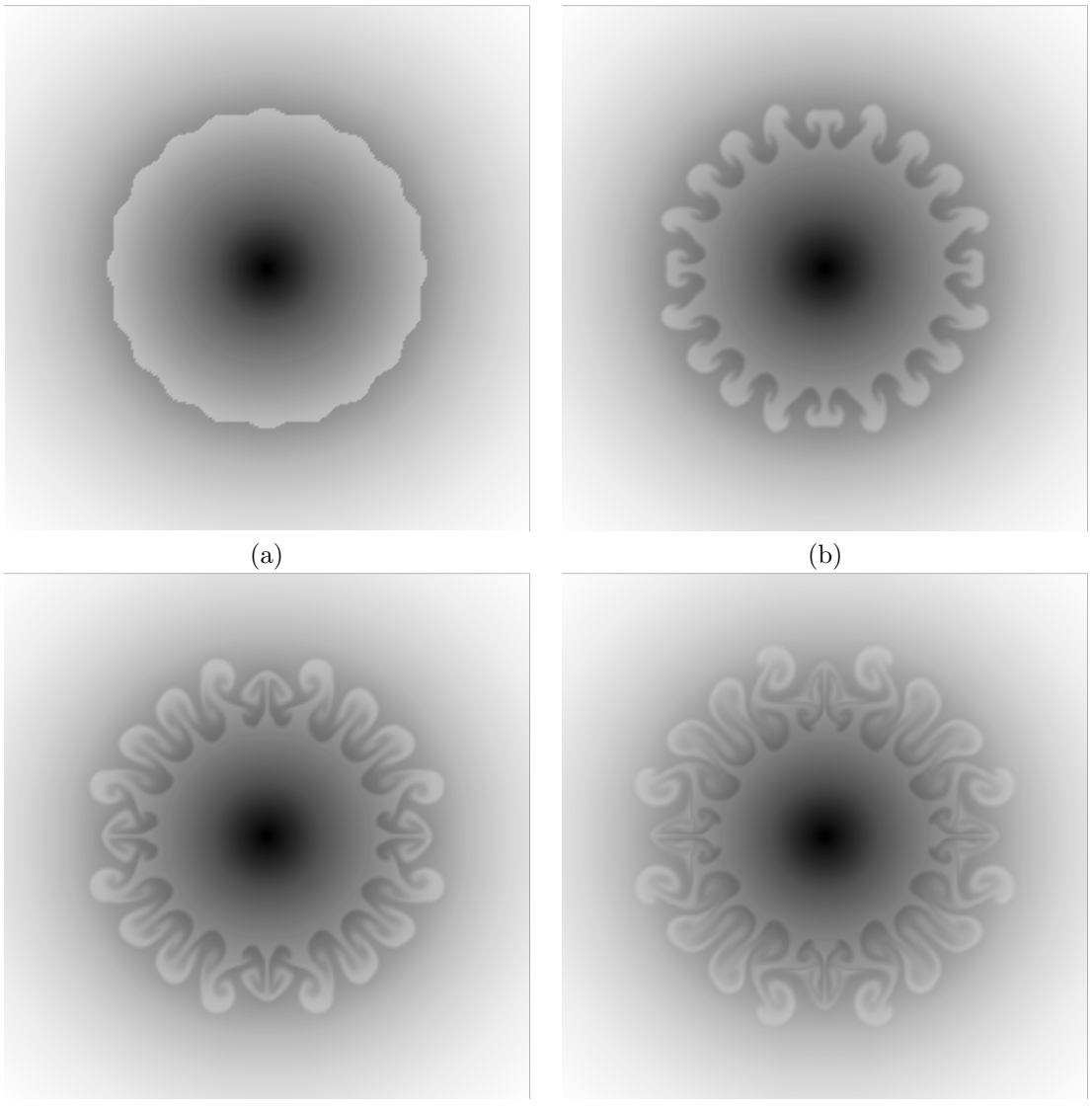

FIG. 8. *Rayleigh-Taylor instability in radial gravitational field obtained with well-balanced scheme. Plots of density at times (a)* $t = 0$*, (b)* $t = 2.9$ *(c)* $t = 3.8$ *(d)* $t = 5.0$*. Darker colour indicates larger values.*